Journal of Power Sources 239 (2013) 572–583

Contents lists available at SciVerse ScienceDirect

Journal of Power Sources

journal homepage: www.elsevier.com/locate/jpowsour

Cycle and calendar life study of a graphite|$LiNi_{1/3}Mn_{1/3}Co_{1/3}O_2$ Li-ion high energy system. Part A: Full cell characterization

Stefan Käbitz [a,c,*], Jochen Bernhard Gerschler [a,c], Madeleine Ecker [a,c], Yusuf Yurdagel [a,c], Brita Emmermacher [d], Dave André [e], Tim Mitsch [e], Dirk Uwe Sauer [a,b,c]

[a] Chair for Electrochemical Energy Conversion and Storage Systems, Institute for Power Electronics and Electrical Drives (ISEA), RWTH Aachen University, Jaegerstrasse 17-19, 52066 Aachen, Germany
[b] Institute for Power Generation and Storage Systems (PGS) @ E.ON ERC, RWTH Aachen University, Germany
[c] Juelich Aachen Research Alliance, JARA-Energy, Germany
[d] ZSW – Zentrum für Sonnenenergie- und Wasserstoff-Forschung Baden-Wuerttemberg, Helmholtzstrasse 8, 89081 Ulm, Germany
[e] Deutsche ACCUmotive GmbH & Co. KG, Neue Strasse 95, 73230 Kirchheim u. Teck (Nabern), Germany

HIGHLIGHTS

- Extended accelerated aging tests on lithium-ion batteries including storage and cycling.
- Detailed analysis of temperature and voltage dependencies of cell aging.
- Correlation of aging results to post-mortem analysis.
- Lifetime prediction based on identified main aging phenomena.
- Alternating aging test under varying SOC.

ARTICLE INFO

Article history:
Received 24 September 2012
Received in revised form
12 January 2013
Accepted 12 March 2013
Available online 26 March 2013

Keywords:
Calendar life
Cycle life
Lithium-ion
Aging
Nickel cobalt manganese
Lifetime prediction

ABSTRACT

This work provides an aging study of a graphite|$LiNi_{1/3}Mn_{1/3}Co_{1/3}O_2$ (NMC) Li-ion pouch cell with a nominal capacity of 10 Ah. By means of resistance and capacity measurements the cell's behavior is tracked over time under consideration of temperature and cell voltage impact. Tests duration was up to 15 months effective testing time. Observed effects and possible aging mechanisms are discussed considering the results from capacity and resistance measurements. The test results are used for a calendar lifetime prediction. In addition to a detailed calendar life study, also cycle life tests are discussed briefly to point out additional aging effects based on cycling. The paper may also serve as data source on aging for further work on battery lifetime modeling and battery diagnostics. Selected cells were taken from the aging tests and were used for a detailed post-mortem analysis (see paper "Part B: Post-Mortem Analysis").

1. Introduction

For a reliable integration of batteries into applications, knowledge about battery aging behavior and especially the achievable lifetime of the battery is indispensable. The influence of different operating conditions on occurring aging phenomena has to be well understood, e.g. for the development of operating strategies, design of battery systems and also business models. Since extended battery tests under real operating conditions are quite time consuming and therefore costly, accelerated aging tests are conducted. If information about occurring aging phenomena is desired, typically a post-mortem analysis has to be conducted [1]. The lack of publications on extensive aging tests of lithium-ion batteries has been reported as a hindrance for the modeling of lithium-ion cell aging phenomena [2]. It is the purpose of this work to provide general information about the aging behavior of a graphite|NMC

* Corresponding author. Chair for Electrochemical Energy Conversion and Storage Systems, Institute for Power Electronics and Electrical Drives (ISEA), RWTH Aachen University, Jaegerstrasse 17-19, 52066 Aachen, Germany. Tel.: +49 241 80 99600; fax: +49 241 80 92203.
E-mail addresses: batteries@isea.rwth-aachen.de, kb@isea.rwth-aachen.de (S. Käbitz).

0378-7753/$ – see front matter © 2013 Elsevier B.V. All rights reserved.
http://dx.doi.org/10.1016/j.jpowsour.2013.03.045

cell for further modeling studies and applications e.g. in battery management systems. Also main features of a test methodology for accelerated aging testing are presented and a mathematical base for lifetime prognosis and lifetime modeling is provided based on Ref. [3]. For several materials extended aging tests were performed in previous works, e.g. for cells with different cathode materials vs. graphite, like $LiCoO_2$ [4,5], NCA [6], NCO [7,8] and LFP [9,10]. Only few publications exist about extensive aging tests with lithium-ion batteries and test matrix sizes comparable to Refs. [9,10]. Though also the NMC cathode is a good candidate for e.g. electric vehicle (EV) applications and is provided by many cell manufacturers for this purpose, only few aging studies concerning this material can be found in literature. The work of Bloom et al. [11], analyzes cycle and calendar life performance of NMC at different temperatures and 60% state of charge (SOC). Ecker et al. [3] used a NMC cathode based cell for modeling of calendar life aging. A large calendar life test matrix and a load profile were used for determination of aging parameters and model verification. However, the focus of Ecker et al. is on modeling and the investigated cells were designed for high power applications up to a C-rate of 20 in hybrid electric vehicles. The work of Bloom et al. did not study the impact of cell voltage on aging. In contrast to Bloom et al. and Ecker et al. the cells investigated in this work are larger and have been built in a process comparable to commercial batch production. They can provide current rates and capacities adequate for a real world application in a battery storage system e.g. for an EV. Apart from these differences, some cells of this work were used for a detailed post-mortem analysis in paper "Part B: Post-Mortem Analysis" [1], allowing a deeper understanding of the occurring aging processes inside this type of lithium-ion battery.

2. Experimental

The tests employ a lithium-ion high energy pouch cell with stacked electrodes, a nominal capacity of 10 Ah and a nominal voltage of 3.6 V. They were semi-automatically custom-manufactured for this study. The anode consists of graphite and the cathode employs $LiNi_{1/3}Mn_{1/3}Co_{1/3}O_2$ (NMC) as active material and aluminum foil as current collector. The electrolyte is constituted of 1 M $LiPF_6$ salt in an organic solvent.

In the following tests the temperature is varied as an impact factor accelerating the rates of both electrochemical cell reactions and parasitic side reactions causing cell aging. Corresponding to other calendar life studies and studies on aging effects [12,13], parasitic reactions of the electrolyte yielding electrolyte decomposition and passivation layer growth at the surface of one or both electrodes are considered as dominating degradation process. The rates of these reactions are strongly related to the electrochemical stability of the different components and additives constituting the electrolyte at various operating conditions. Based on these considerations, a test matrix as depicted in Table 1, has been designed. The choice of test temperatures has been made with respect to specifications of the cell manufacturer, regarding the thermal stability of active masses and electrolyte. For achieving a higher degree of repeatability in the tests, every working point of the matrix is tested as a batch consisting of two or three cells. Before starting the tests, these batches were selected with respect to similar actual capacities and resistances for minimizing the impacts of statistical spreads. During the tests, the cells marked with "CV" are stored in ovens or climate chambers at elevated temperatures and at constant voltage. The others marked with "OC" were stored at open circuit conditions. For keeping the voltage constant, every single cell is connected to a power supply unit. Voltages are derived from open circuit voltage (OCV) measurements at test temperature of $T = 25\ ^\circ C$ as depicted in Fig. 1. The state of charge (SOC) and depth of discharge (DOD) in this work is related to the nominal capacity of 10 Ah.

Table 1
Calendar life test matrix. Two different kinds of calendar life tests were performed: OC – storage of cells at open circuit conditions, and CV – using a constant voltage source to ascertain a constant potential during the test. Numbers indicate the amount of cells per test.

	$T = 25\ ^\circ C$	$T = 40\ ^\circ C$	$T = 50\ ^\circ C$	$T = 60\ ^\circ C$
20% SOC, 3.59 V		2xCV/2xOC		3xCV
50% SOC, 3.72 V	3xCV	3xCV/3xOC	3xCV	3xCV
80% SOC, 3.96 V		2xCV/2xOC		3xCV
90% SOC, 4.06 V		2xCV		2xCV
100% SOC, 4.19 V	3xCV	2xCV/2xOC		3xCV

In addition to calendar life aging tests also cycle life tests were performed at 1 C-rate and $T = 40\ ^\circ C$ with 10% DOD around a mean SOC of 95%, 5%, 50% and 50% DOD around 75% mean SOC at this temperature. In test reaching either end of discharge voltage (EODV) of 3.0 V or end of charge voltage (EOCV) of 4.2 V the cycling was started at those voltages with a charge or discharge. In addition to these tests, cycles between EODV and EOCV were tested at $T = 25\ ^\circ C$, 40 °C and 60 °C at 1 C-rate. Though not reaching the full capacity due to ohmic, kinetic and diffusion based voltage drops, these tests are referred to as "full cycle" in the following. One cycle between EOCV and EODV at $T = 40\ ^\circ C$ leads to a discharged capacity of approximately 9.5 Ah per cycle directly after begin of test (BOT) and 7.5 Ah near end of test (EOT). All cycle life tests were conducted with air cooling and heat sinks on both sides of the pouch cells in climate chambers or ovens. The ambient temperature was controlled to keep the surface temperature of the cell at the desired test temperature with a maximum difference of 2 K.

To investigate aging and to determine the actual cell status, a reference parameter test (RPT) is carried out at BOT, at EOT and in intervals of 6 weeks in between. The RPT is depicted in Fig. 2. It consists of a static capacity test at standard conditions ($T = 25\ ^\circ C$) including a 1 C-rate discharge of retention capacity to EODV, a standard charge (1 C-rate constant current charge to EOCV, constant voltage charge at EOCV until current has decreased below 0.05 C-rate) and a 1 C-rate discharge of the fully charged cell to EODV for determining the actual capacity C_{act}. Furthermore it contains determination of charge and discharge resistances using a current pulse at different depths of discharge. In context of this work, it employs an 18 s 4 C-rate discharge pulse followed by a 40 s rest period and a 10 s 3 C-rate charge pulse also followed by a 40 s rest period. Resistances are determined between 90% and 10% SOC.

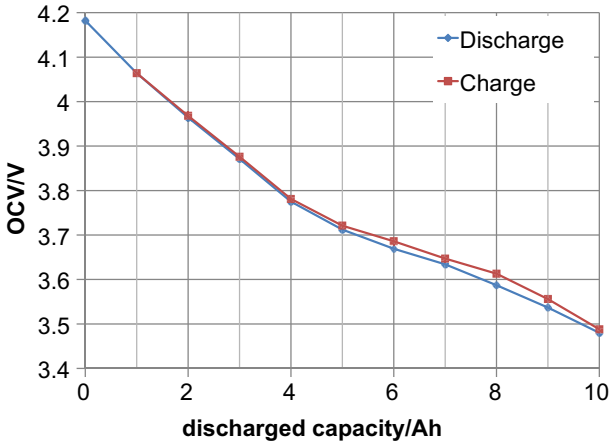

Fig. 1. Open circuit voltage (OCV) plotted vs. discharged capacity for the investigated graphite|NMC Li-ion high energy cell at $T = 25\ ^\circ C$ after charge and discharge showing a small hysteresis at low states of charge.

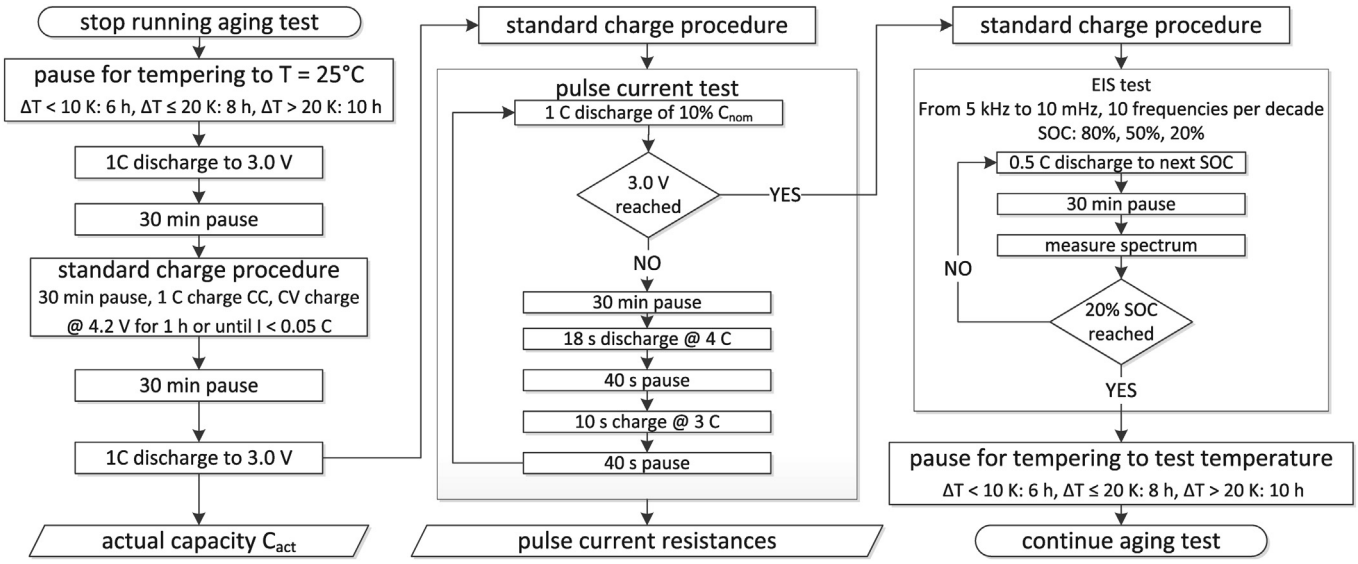

Fig. 2. Test procedure of the reference parameter test (RPT) applied at begin of test, end of test and every 6 weeks in between.

In this work the two key values describing the cell status are the actual capacity C_{act} and the 10 s discharge resistance R_{act} at 50% SOC. The resistance is calculated by the difference between the voltage before the 4 C-rate discharge pulse and after 10 s during the pulse, as depicted in Fig. 3, divided by the current during the discharge pulse. All values in this work are mean values of the two or three tested cells.[1] Every cell was also characterized via electrochemical impedance spectroscopy (EIS) at each RPT. A detailed analysis of the impedance spectra obtained during the aging tests will be given in a separate publication.

3. Results and discussion

3.1. Variation of temperature in calendar life tests

For outlining temperature impact on degradation, actual capacity and resistance are plotted vs. time for storage at a constant cell voltage of 3.72 V, which is equivalent to 50% SOC, and four ambient temperatures (T = 25 °C, 40 °C, 50 °C, 60 °C). Their evolutions over time, which are depicted in Fig. 4(a) and (b), are normalized to conditions at BOT. The diagrams show average values of the cells constituting a test scenario and also the values for each individual cell, to illustrate the variance in between the specimen. As expected an increase of storage temperature causes a significant acceleration of capacity decline and resistance increase, which is especially high for T = 60 °C. The resistance increase shows a similar behavior as the capacity decline, except for the test at T = 40 °C. The resistance increase appears lower for this temperature compared to the increase of capacity degradation between T = 25 °C and T = 40 °C. Part of this phenomenon has to be accounted to the problem, that the resistance of the cells is rather small (R_{act} is approximately 4.7 mΩ at BOT). Furthermore even slight changes in temperature of 2 K from RPT temperature of T = 25 °C, as defined in Section 2, show a change of the resistance value of approximately 5%. Thus resistance values are more prone to measurement errors. Anyway the control of the temperature chambers was normally more exact than the specified 2 K. Nevertheless it cannot be excluded that single data points might show deviation because of these problems.

Identification of main aging mechanisms related to single processes is hardly ever possible without carrying out post-mortem analysis, especially for checking the electrochemistry of the single electrode. The interactions between the components of a full cell system are too complex, to allow a separation into single aging effects by RPT as used in this work. Results from post-mortem analysis [1] indicate that the observed capacity fade is mostly due to loss of active lithium at the anode, probably due to continuous solid electrolyte interface (SEI) formation. Changes in porosity and weight of the samples reveal the evolution of deposition products in the porous structure of the anode, indicating electrolyte decomposition. Using inductively coupled plasma optical emission spectroscopy (ICP-OES) showed, that most of the lithium lost in the cathode was deposited during aging on the anode [1]. Finding most of the lost reversible lithium on the anode side also points to a SEI deposition reaction as main lithium loss mechanism. This fits quite well to the observed phenomena in the RPTs. Nearly all aging curves in this work show a stronger degradation in the beginning and an apparent linear behavior after a longer period of time. Usually this behavior is accounted to the growth of the SEI on the anode. Since the potential of lithiated graphite electrodes is outside the stability window of the electrolyte, a stable SEI is crucial for cell

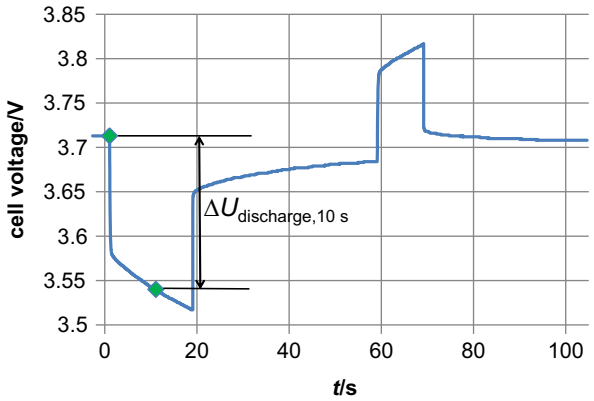

Fig. 3. Cell voltage vs. time during pulse current test. The rhombi mark the voltage values used for calculation of the 10 s discharge resistance. All shown resistances R_{act} in this work are recorded at 50% SOC and t = 10 s.

[1] The spread between the parameters of each cell can be seen in Fig. 4(a) and (b).

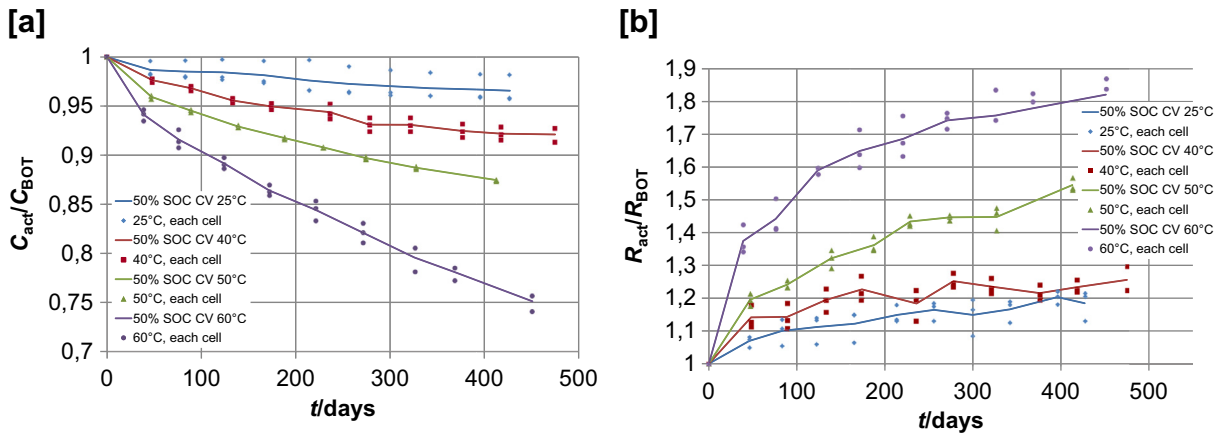

Fig. 4. Actual capacity C_{act} (a) and discharge resistance R_{act} (b) vs. time at different temperatures and 50% SOC. All values are normalized to conditions at begin of test (BOT). Averaged values and values for each individual cell are shown.

performance [13–16]. By growing in thickness, the SEI is protecting the electrolyte more effectively from further reduction. The reactants for side reactions are supposed to diffuse through the SEI, leading to a square root of time shaped degradation due to SEI thickness increase [17]. Since the lithium-ions have to pass through the SEI, a resistance increase is observed related to thickness.

3.2. Variation of cell voltage in calendar life tests

Figs. 5 and 6 depict the evolution of actual capacity (a) and resistance (b) vs. time at test temperatures of $T = 40\,^{\circ}C$ and $T = 60\,^{\circ}C$ with various SOC. The characteristics of the capacity fade at CV in Fig. 5(a) appear to have a more complex dependency on voltage than on temperature. In fully charged state (4.18 V, 100% SOC) at $T = 40\,^{\circ}C$ the cells age very fast, especially within the first few weeks of storage, losing more than 20% of capacity in less than a year under test. A visual inspection of cells stored at 4.18 V indicated a moderate gas evolution within the pouch packs. Cell voltages equal to or less than 4.06 V (90% SOC) show a stabilization of the system. Between 50% SOC and 80% SOC there is only a difference of approximately 3% in capacity decrease after 170 days. Unfortunately the 80% CV ended after a period of 170 days because of a cell damage. The capacity decrease of the 90% SOC test looks similar to the test at 80% SOC, but in the first RPT a different aging behavior is observed. The reason might be a different BOT time, since both 90% SOC tests were started approximately five months later than the other tests described in this work. The cells used in the delayed tests were used for only few preceding test cycles and then stored at room temperature. At BOT they showed no significant change in resistance and capacity values compared to those after first checkup, after the cells were supplied to the test facilities. The 20% SOC test shows a completely different behavior with an increase of capacity at BOT, keeping the relative capacity above 100% for 300 days of testing.

The comparison between OC and CV in Fig. 5 shows a different aging behavior only at 100% SOC. The other capacity curves show no significant difference between OC and CV storage conditions. After a period of approximately 200 days, the capacity offset seems to remain nearly constant. The 100% OC test was accidently set to 20% SOC after the fourth RPT (200 days) and seventh RPT (361 days) for 6 weeks respectively. In both cases a capacity recovery (2.9% and 1.5% respectively) is observed. Looking at self-discharge of the cells, the 100% OC test shows a drop of voltage between the RPTs of 100–180 mV. For comparison, the voltage drop of the 20% SOC test between each RPT due to self-discharge is about 20–30 mV. It seems the voltage of 4.18 V at 100% SOC leads to potentials near the stability window of the electrolyte. If the voltage is kept high, as in a CV test, the battery voltage and the side reaction rate are kept higher in comparison to an OC test. By self-discharge the OC tests can drop to potentials, where the electrolyte is more stable, decreasing the capacity fades. At lower SOC the electrolyte is stable anyway, so not only the self-discharge rate is low, but also the influence of cell voltage decrease is negligible, leading to similar behavior of OC and CV tests.

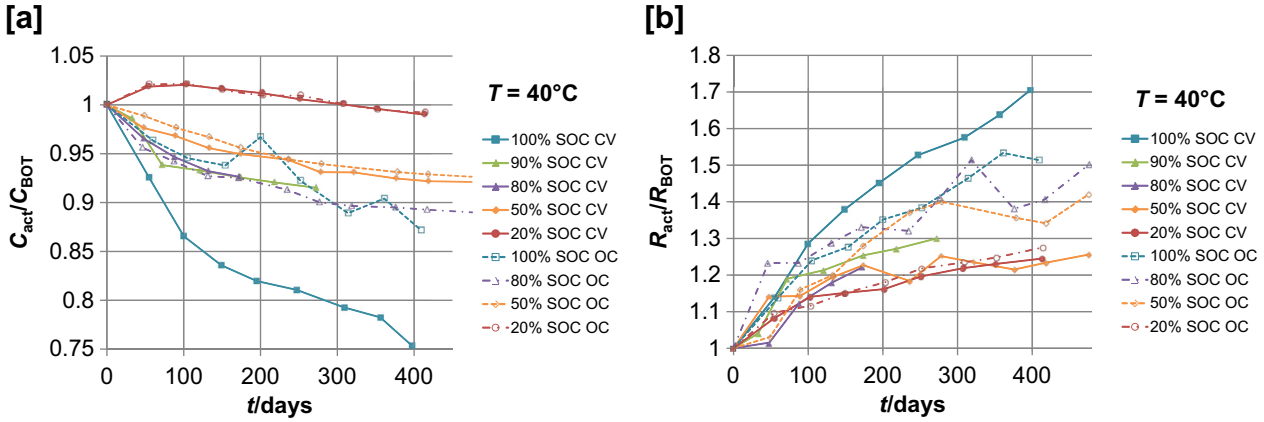

Fig. 5. Actual capacity C_{act} (a) and discharge resistance R_{act} (b) vs. time at different SOC and $T = 40\,^{\circ}C$. Solid lines with filled markers show tests at constant voltage (CV). Dashed lines with hollow markers show tests under open circuit (OC) conditions. All values are normalized to conditions at begin of test (BOT).

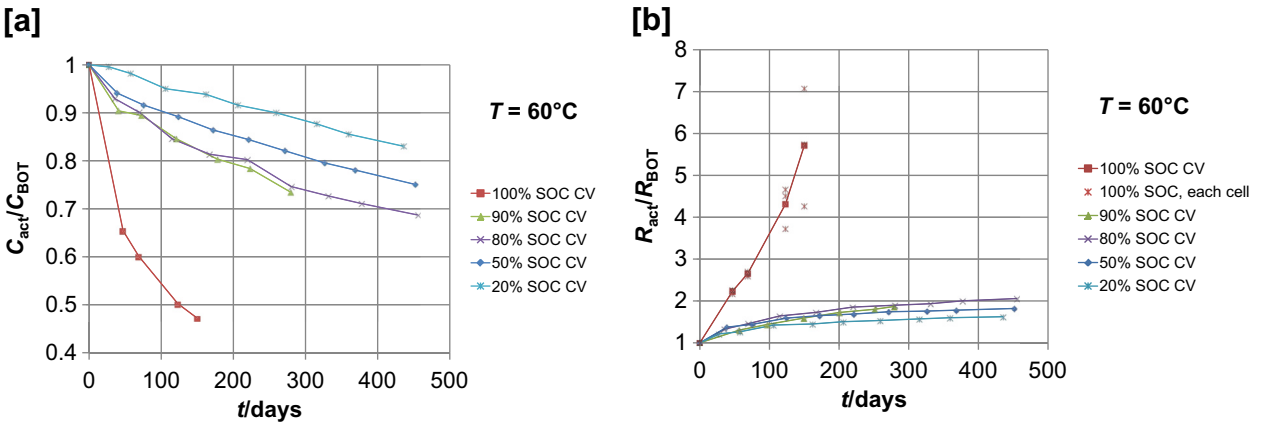

Fig. 6. Actual capacity C_{act} (a) and discharge resistance R_{act} (b) vs. time at different SOC and $T = 60\,^{\circ}C$. All values are normalized to conditions at begin of test (BOT). (b) Shows in addition data points for each cell at 100% SOC, exposing strong deviations in between the three cells.

In the resistance curves in Fig. 5(b) a slightly different behavior can be observed. While the OC and CV test behavior at 100% SOC and 20% SOC can be explained by the aforementioned model, the OC tests at $T = 40\,^{\circ}C$ at 80% SOC and 50% SOC show some resistance scattering and a higher resistance increase than the CV tests. This is quite unexpected, but in the final analysis no alternative explanations were found based on the test data observed in this study. These OC vs. CV resistance aging effects have to be studied in more detail in further studies. Furthermore the resistances for both 20% SOC and 100% SOC tests show a different behavior compared to capacity. Although a capacity increase can be observed at 20% SOC, the resistance increases in this test scenario. During the change to 20% SOC in the 100% SOC OC test, the capacity recovers, but also here the resistance does not decrease at the same time (Fig. 5(b)). Nevertheless the resistance increase is smallest at 20% SOC CV and highest at 100% SOC CV. The 100% SOC OC test might show a slight influence of the two time periods at 20% SOC, but at least the influence is quite small and within the range of the error of the resistance measurement. Altogether the resistance increase seems to be less sensitive to the cell voltage level than the capacity loss.

The capacity tests at $T = 60\,^{\circ}C$ (Fig. 6(a)) behave quite as expected, since their aging behavior is increased in rate due to the higher temperature. While the 100% SOC test shows an extreme decrease of capacity again, 80% SOC and 90% SOC behave nearly identical. The resistances in Fig. 6(b) correspond quite well to the capacity decrease. The 20% SOC test shows no capacity increase any more, but an unusual shape for capacity decline, which is also discussed in more detail later in Section 3.5.

3.3. Cycle life

The results of the cycle life tests analyzed in this work are depicted in Figs. 7 and 8. All tests run at 1 C-rate, leading to a throughput of approximately 20,000 discharged Ah after 200 days, which equates to 2000 equivalent full cycles. The tests discussed in this work are shown in Table 2. Within this study several additional cycle life tests have been performed, but they will be discussed in a separate publication.

Compared to the calendar life tests a significant influence, especially of the full cycles, can be derived. In Fig. 7(a) the 10% DOD cycles show little to no added influence on capacity decrease compared to the corresponding calendar life tests. In contrast 50% DOD and full cycles differ significantly from calendar life aging. From the results depicted in Fig. 7(b) no clear dependency for the resistance can be derived. All cycle tests at $T = 40\,^{\circ}C$ show a similar behavior with only slight dependency on mean SOC and no clear dependency on DOD.

Fig. 8(a) shows the influence of full cycles at different cell temperatures on capacity. In difference from Ref. [11] all cycle life tests show a higher capacity decline than the storage tests with the

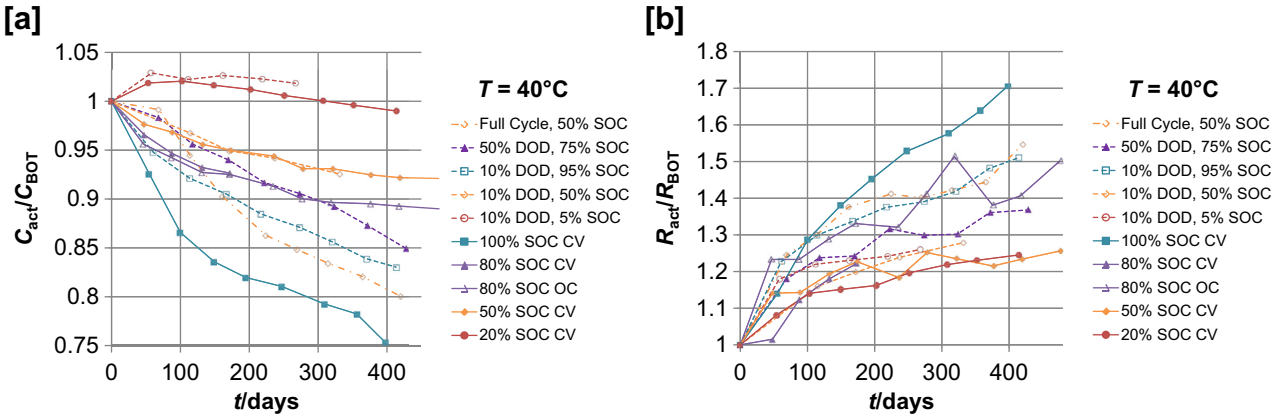

Fig. 7. Actual capacity C_{act} (a) and discharge resistance R_{act} (b) vs. time for cycle life tests at 1 C-rate at $T = 40\,^{\circ}C$. Tests were performed at different DOD around different mean SOC. Dashed lines show the cycle life tests. Selected calendar life tests equal or near to the mean SOC are depicted for comparison and drawn as continuous lines. All values are normalized to conditions at begin of test (BOT).

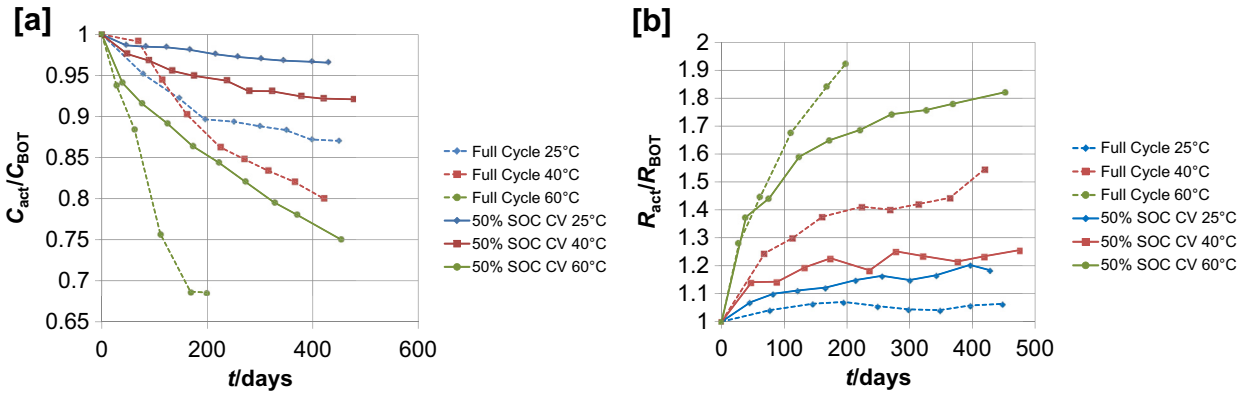

Fig. 8. Actual capacity C_{act} (a) and discharge resistance R_{act} (b) vs. time for cycle life tests at 1 C-rate at different temperatures. Dashed lines show the cycle life tests. Selected calendar life tests equal to the mean SOC of the cycle tests are depicted for comparison and drawn as continuous lines. All values are normalized to conditions at begin of test (BOT).

corresponding mean SOC. At $T = 25\,^{\circ}C$, after approximately 400 days of cycling, the capacity decline is about factor 3.86 higher compared to the CV calendar life test at the corresponding mean SOC of 50%. For $T = 40\,^{\circ}C$ after the same time period this factor is 2.6 and for $T = 60\,^{\circ}C$ after 170 days it is factor 2.3.

Resistances in Fig. 8(b) show a complex dependency on temperature. The RPT after 400 days of cycling at $T = 25\,^{\circ}C$ shows only 6% increase of resistance while the corresponding calendar life test at 50% SOC CV shows an increase of about 20% after 400 days. At the same time and at $T = 40\,^{\circ}C$ cycle life resistance is approximately 25% higher than the calendar life resistance. At $T = 60\,^{\circ}C$ the test ends already after 200 days of cycling. At that time the cycle life resistance is also approximately 25% higher than in the corresponding calendar life test. It is remarkable, that the resistance increase at $T = 25\,^{\circ}C$ is smaller than in the corresponding calendar life test, since the capacity fade is stronger. This behavior points to an additional effect that has to take place besides a SEI formation which is enhanced by high temperature and high voltages. Post-mortem analysis [1] results on cycling highlight a possible explanation for the behavior of the resistance curves in Fig. 8(b). On the one hand the electrode volume increases during cycle life tests, on the other hand the mass increases especially at high temperature, which is ascribed to SEI deposition. Whereas the first effect increases porosity the latter decreases it. What is experimentally observed is a larger porosity increase at low temperature than at high temperature. At higher temperatures, the deposition reaction counteracts the volume expansion, leading to a decrease of porosity thus to higher resistance values.

3.4. Analysis of temperature dependencies

For more in-depth analysis of temperature impacts on aging, an Arrhenius plot (Fig. 9) is analyzed for both capacity decline and resistance rise over time as done in the work of Liaw et al. [18] for a graphite|1.2 M $LiPF_6$ ethylene carbonate (EC):ethyl methyl carbonate (EMC)(w:w = 3:7) $|Li_xNi_{0.8}Co_{0.15}Al_{0.05}O_2$ cell. Though equipped with a different cathode material, their cell consists of similar electrolyte and anode materials. The basis for this analysis is the well-known Arrhenius equation given in equation (1):

$$A = A_0 \cdot \exp\left(-\frac{E_a}{RT}\right) \tag{1}$$

It describes the rate A of a thermally activated process depending on A_0, which corresponds directly to the process, the activation energy E_a representing the energy barrier for the thermal activation process, the universal gas constant R and the absolute temperature T in degrees Kelvin. E_a is derived via linear regression from the slope of an Arrhenius plot. It is supposed to be linked to the rate determining step in the thermally activated process chain yielding to cell degradation. Fig. 9(a) depicts the logarithmic capacity decline normalized to the actual capacity at BOL versus reciprocal temperature at certain time intervals in days. Data points are taken from the calendar life matrix at 50% SOC CV and corresponding temperatures. Every dot represents the average capacity loss of two or three cells. Since the RPTs did not occur at the same time for all tests, linear interpolation was used when necessary. The activation energies E_a resulting from linear regression and the coefficient of determination R^2 of the regression for capacity loss and resistance increase are shown in Table 3. The regression works quite well for the capacity decline. For the resistance values some imprecise regression curves are calculated. Especially in the beginning the regression curves fit quite well. Near to the EOT regression curve fits become worse. Possibly this is indicating that different aging processes are occurring, but this phenomenon might also be based on measurement errors. The latter is quite likely, because the change in slope in Fig. 9(a) begins after 210 days corresponding to an unexpected pronounced resistance decrease at $T = 40\,^{\circ}C$, which can be seen in Fig. 4(b). Anyway most curves fit quite well, so the assumption of Arrhenius type behavior appears justified for both resistance increase and capacity decline.

Fig. 10 displays the different E_a values resulting at the different times taken from the (interpolated) RPTs. For the capacity loss a mean activation energy of $E_a = 43.6$ kJ mol^{-1} has been derived. These values are at least in parts nearly equal to the values determined by Liaw et al. Namely the C/1 capacity from BOT until 13 weeks of test (E_a between 55 kJ mol^{-1} and 42 kJ mol^{-1}) and, and the C/25 capacity in between 17 and 21 weeks of aging (43 kJ mol^{-1}, first three RPT are around 30 kJ mol^{-1}). In contrast to the work of Liaw et al. [18], no significant increase in E_a can be observed over time. Following their argumentation, this means there is only a single-stage process for capacity decline in case of this cell. The resistance increase leads to mean activation energy of

Table 2
Cycle life tests discussed in this work. Full cycles were performed at constant current in between EODV and EOCV. All other tests were cycled at constant current and a DOD based on the nominal capacity (see Section 2).

Range	Full cycle	Full cycle	Full cycle	100–50% SOC	90–100% SOC	45–55% SOC	0–10% SOC
Temperature	25 °C	40 °C	60 °C	40 °C	40 °C	40 °C	40 °C
C-rate	1	1	1	1	1	1	1

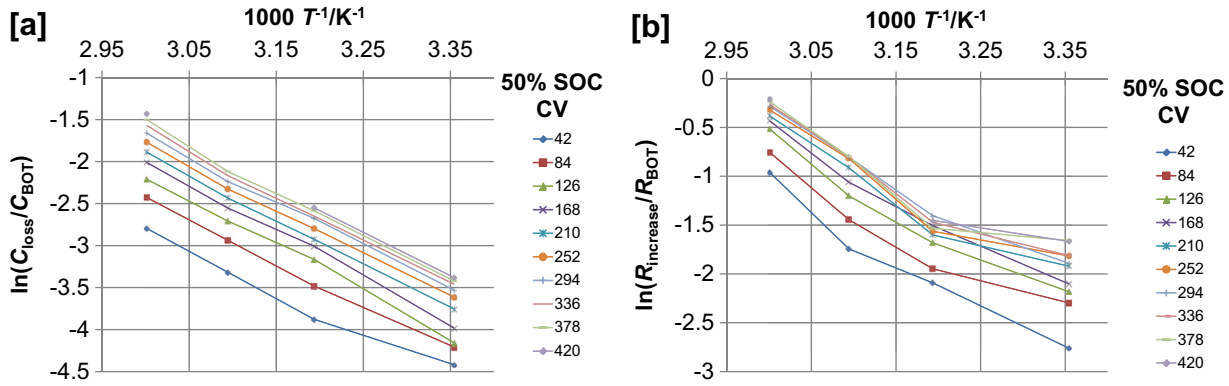

Fig. 9. Logarithmic capacity loss (a) and resistance increase (b) vs. inverse ambient temperature. Set of curves show different points of test time in days. All values are normalized to conditions at begin of test (BOT). Cells used for this test were taken from the calendar life matrix at 50% SOC CV and corresponding temperatures.

E_a = 36.9 kJ mol^{-1}. The value determined by Liaw et al. is E_a = 32.2 kJ mol^{-1} after 12 weeks of aging. However Liaw et al. determined the dependencies at 80% SOC and with a different cathode material. Furthermore the cells at $T = 25$ °C in the work of Liaw et al. were excluded from analysis because of untypical behavior. These differences and of course the differences in the used cell materials are supposed to have a part in the observed deviations in the activation energies. Anyway the determined Arrhenius parameters for cell aging are at least in parts quite similar and do not contradict the hypothesis of SEI deposition reactions on the anode as main aging mechanism.

3.5. Analysis of voltage dependencies

For a further analysis of the voltage influence on cell aging, the charts in Figs. 11 and 12 are introduced. They depict the capacity loss (a) and resistance increase (b) vs. cell voltage for $T = 40$ °C and $T = 60$ °C respectively. The set of curves represent different times at or in between the RPTs. Linear interpolation was used for calculation of parameters if time of the RPT was different. At 80% SOC and $T = 40$ °C, in Fig. 11(a), the OC curve was used as an approximation for the CV curve. Both tests behave quite similar concerning the capacity decrease (see Fig. 5(a)) and this way more data points are available, since the runtime of the OC test is longer. All other depicted data in both figures is taken from CV tests.

Fig. 11(a) shows that between SOC of 50%, 80% and 90%, the difference in capacity decline is small. E.g. after 236 days in test, 5.6% of capacity has been lost at 50% SOC, 8.6% at 80% SOC and 8.1% at 90% SOC. In contrast to this, 18.7% of the capacity has been lost at 100% SOC at that time. In Fig. 11(b) between 20% and 80% SOC no

Table 3
Results from Arrhenius plot analysis obtained via linear regression. The R^2 values describe the quality of linear regression of the logarithmic capacity loss vs. inverse temperature.

Days	R^2 capacity	Activation energy (E_a/kJ mol^{-1})	R^2 resistance	Activation energy (E_a/kJ mol^{-1})
42	0.9818	38.2549	0.9639	40.3964
84	0.9972	41.9624	0.9241	35.3279
126	0.9962	45.5543	0.9589	38.1895
168	0.9974	45.9628	0.98	38.3607
210	0.999	43.6348	0.9325	36.6489
252	0.9983	42.9527	0.9131	36.0146
294	0.9973	43.3117	0.9728	37.9969
336	0.9966	43.9005	0.9385	36.7709
378	0.9961	44.5021	0.863	33.947
420	0.9989	45.9983	0.8924	34.872

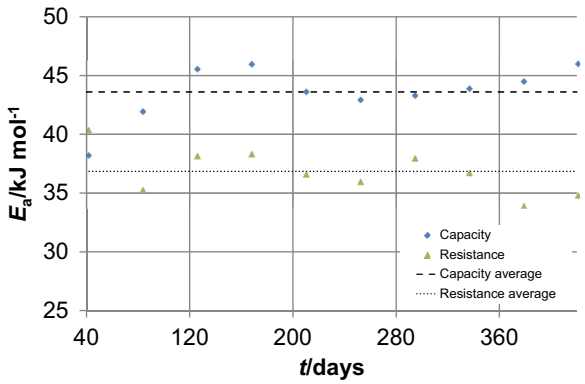

Fig. 10. Activation energy E_a of processes correlated to capacity decline and resistance increase plotted vs. test time in days.

clear impact of the SOC on resistance increase can be seen. The degradation starts to increase slightly at 90% SOC and grows rapidly at 100% SOC. The aging behavior illustrated in Fig. 12(a) and (b) is basically identical, but degradation is higher because of Arrhenius type behavior. Since the scattering of the resistances is lower than at $T = 40$ °C and the overall degradation of the test at $T = 60$ °C and is higher, a trend in resistance increase is visible.

A very interesting point is the aging behavior at 20% SOC. At $T = 40$ °C it shows an increase of the capacity not only in the beginning, but also during the 100% SOC OC test (Fig. 5(a)), which has been stored twice at lower SOC as described in Section 3.2. Since there is a discharge and a charge before every capacity test, this capacity increase effect has to last for some time. On the other hand, looking at the 100% SOC OC curve, it appears that the gain in capacity tends to be extinct after another storage period of 100% SOC. At the first look this effect of capacity increase at 20% SOC is not observable at $T = 60$ °C. In any case the aging curve in Fig. 6 looks unusual at this temperature, since the capacity decline after BOT is lower than at the other SOC. It is supposed that also in this test at $T = 60$ °C a tendency for capacity increase exists due to the low SOC, but is overlapped by the high capacity decrease caused by the higher temperature. To check this connection between the observed curve shape at $T = 60$ °C and the effect at $T = 40$ °C it is assumed, that 50% SOC and 20% SOC show an identical aging concerning capacity decline at both temperatures. Hence the difference between the tests is the gain of capacity due to the storage at low SOC. Using linear interpolation this difference is calculated for the tests at $T = 60$ °C. Afterward this calculated difference is added as gain to the $T = 40$ °C 50% SOC CV test. The result is the curve

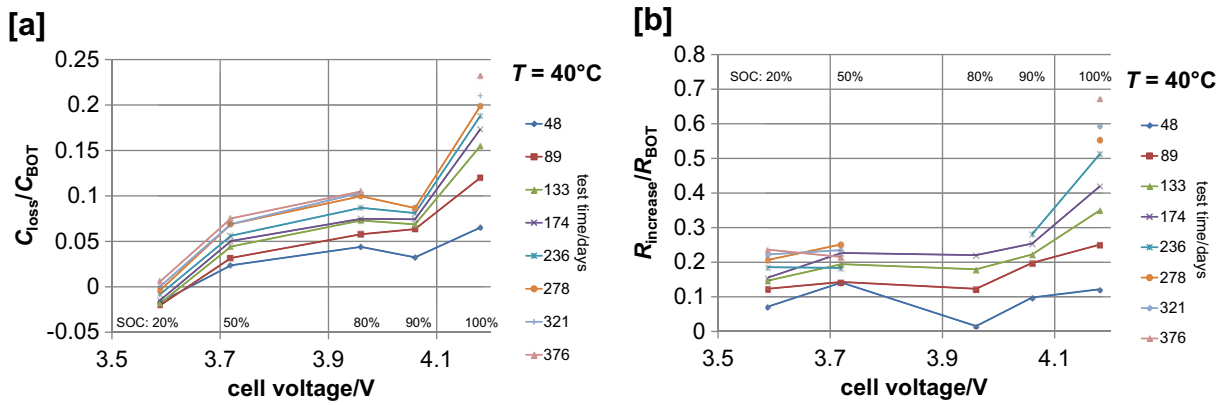

Fig. 11. Capacity loss (a) and resistance increase (b) vs. cell voltage at $T = 40$ °C. Set of curves show different points of test time in days. All values are normalized to conditions at begin of test (BOT). Lines after 174 days are interrupted, because the 80% SOC test was aborted. Furthermore after 272 days the 90% SOC data ends, because the test was started later (see Section 3.2).

depicted in Fig. 13 as "Calculated 50–20". The remaining error between measured and calculated curve is rather small, indicating that this process might indeed be temperature independent. The reason for this effect is unknown to the authors, no hints in literature for this effect are known to the authors either.

It is harder to find a function for the capacity decline and the resistance increase in dependency of the voltage compared to the temperature. In order to give access to the aging parameters e.g. for modeling and also for further clarification of the voltage dependency, Table 3 gives an overview of the voltage impact on loss of capacity and resistance gain. Values were calculated based on the last set of curves, where all tests were available. This is 84 days for $T = 60$ °C. Nearest value at 89 days was chosen for $T = 40$ °C. Since 20% SOC at $T = 40$ °C gained capacity, the values were related to 50% SOC.

In literature often an exponential function is suggested for voltage dependencies of electrochemical processes [3]. In this case there is no evidence for an exponential behavior. A nearly stepwise voltage dependency, as expected if the anode is the main voltage dependent aging factor [13], is also an option for interpretation of the collected data in this work. The graphite potential against Li/Li+ is partly stepwise in shape and shows only small decrease in voltage after reaching the 2L stage with ongoing lithiation above $Li_{0.2}C_6$ [19]. This may cause only small differences in the anode potential influencing the aging, though the SOC and also cell voltage changed significantly [13]. Anyway, even if the anode side is the main reason for capacity loss, the cathode side is also likely to account to aging performance. Especially at high SOC and high temperatures Broussely et al. anticipate electrolyte oxidation at the cathode leading particularly to resistance increase [13]. In fact, the post-mortem analysis of the present cells [1] shows distinct capacity loss for the cathode material for high SOC and high temperature, where SOC has a higher impact than temperature. Since slight gas evolution under high temperature and high voltage conditions has been observed, it cannot be excluded yet that the drastic aging at 100% SOC and high temperatures is also due to cathode side phenomena. As the OC tests at 100% SOC and $T = 40$ °C show, the degradation significantly decreases if the cell voltage is allowed to fall about 100 mV due to self-discharge in between the RPT. This behavior might hint to an additional aging effect occurring at 100% SOC, but could also be a very fast exponential acceleration of the formerly described aging effects at the anode [20]. Finally the different processes have to be announced again in later works, taking also into account the electrochemical impedance spectra and the results of the post-mortem analysis.

3.6. Alternation – storage at varying cell voltage

In applications and under typical operating conditions storage voltages will vary depending on specific load profiles. Motivated by this fact, a storage test with varying cell voltages at CV conditions was started at $T = 40$ °C. Fig. 14 shows the applied SOC test profile.

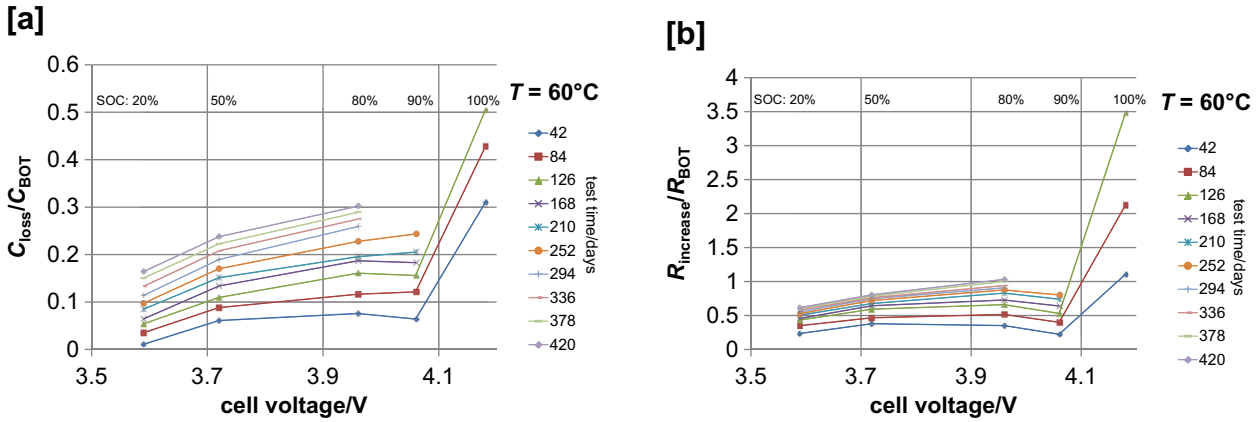

Fig. 12. Capacity loss (a) and resistance increase (b) vs. cell voltage at $T = 60$ °C. Set of curves show different points of test time in days. All values are normalized to conditions at begin of test (BOT).

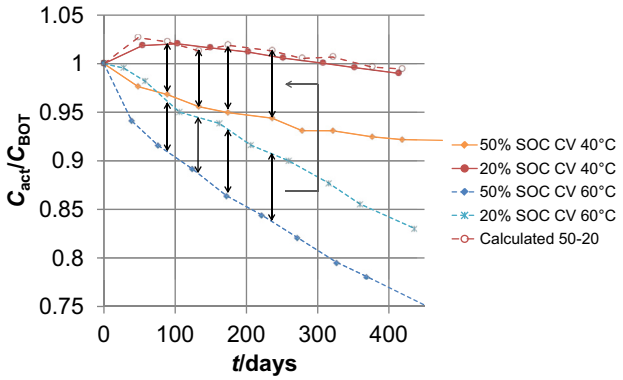

Fig. 13. Analysis of losses at 20% SOC. The difference of actual capacity between 50% SOC and 20% SOC at $T = 60\,^{\circ}C$ is added to the 50% SOC at $T = 40\,^{\circ}C$ capacity. The "Calculated 50–20" curve is the result.

From Fig. 15(a) it can be observed, that whenever going from higher to lower voltage a capacity recovery takes place, similar to the 100% OC test at $T = 40\,^{\circ}C$. Going from lower to higher voltage, capacity decline accelerates again and the already known capacity recovery effects seem to vanish. The resistance in Fig. 15(b) shows no clear dependency on SOC. 20% SOC seems to be somehow beneficial to resistance increase, all other SOC lead to resistance increase. Nevertheless, the overall resistance of the test compared to other storage tests appears quite low, especially at the beginning of the test. Taking into account the small dependency of resistance increase on SOC (see Section 3.5), also scattering of values might be a problem for interpretation of the curve. Similar to 90% SOC, BOT for the alternation test was six months later than the other test, which might explain the strong capacity decline at BOT compared to the 50% SOC CV test in the plot due to earlier storage conditions. However just as the 90% SOC tests, a comparison to initial values did not show significant capacity decline or resistance increase at BOT.

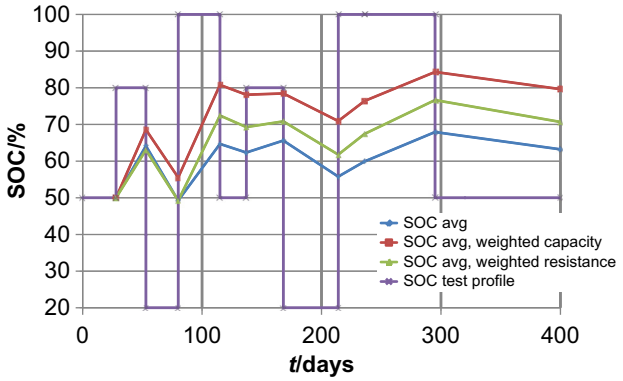

Fig. 14. Alternation test profile and calculated resulting arithmetic average SOC and average weighted SOC for resistance increase and capacity loss.

Though the complex behavior at each time step of this test cannot be explained by a simple model, a method is discussed in the following to approximate the overall aging of the alternation test. To take into account the voltage dependency, the values derived in Section 3.5 are used to determine the average (avg) weighted SOC during the alternation test. This weighted average SOC is supposed to correspond to the SOC of a calendar life CV test, showing the same grade of aging. The resulting average weighted SOC is calculated via equation (2).

$$\mathrm{SOC}_{\mathrm{avg,weighted}} = \frac{\sum_i a(\mathrm{SOC}) \cdot \mathrm{SOC}_i \cdot t_i}{\sum_i a(\mathrm{SOC}) \cdot t_i} \tag{2}$$

a(SOC)is taken from Table 4 at $T = 40\,^{\circ}C$ and t_i is the period of time at SOC_i. Resulting average weighted SOC is shown in Fig. 14 for weighting with capacity and resistance parameters. Also the arithmetic mean value is shown, corresponding to an $a(\mathrm{SOC}) = 1$. Since this rather simple approximation is not supposed to take into account the effect of capacity increase at low SOC, a(20% SOC/50% SOC) is set to one. Calculation predicts a capacity fade at 400 days corresponding to a test at 80% SOC CV. Fig. 15(a) shows the comparison of 80% OC capacity, which is similar to 80% CV mentioned before, and alternation behaving the same way. Though ignoring former cell history, after 400 days both tests show nearly the same capacity decline. Since the capacity gain at low SOC does not seem to be permanent at higher SOC, the capacity prediction using a weighted SOC is quite correct at different time points with higher previous SOC.

The observed capacity gain phenomenon might be an error source for online calculation of actual capacities in battery management systems, since the gain achieved at 214 days is in parts still persistent even after 22 days of storage at 100% SOC. For long-term lifetime prediction, with a profile including higher SOC, the simple approximation derived in this chapter could be sufficient. In any case, the resistance curves behavior could not be predicted with

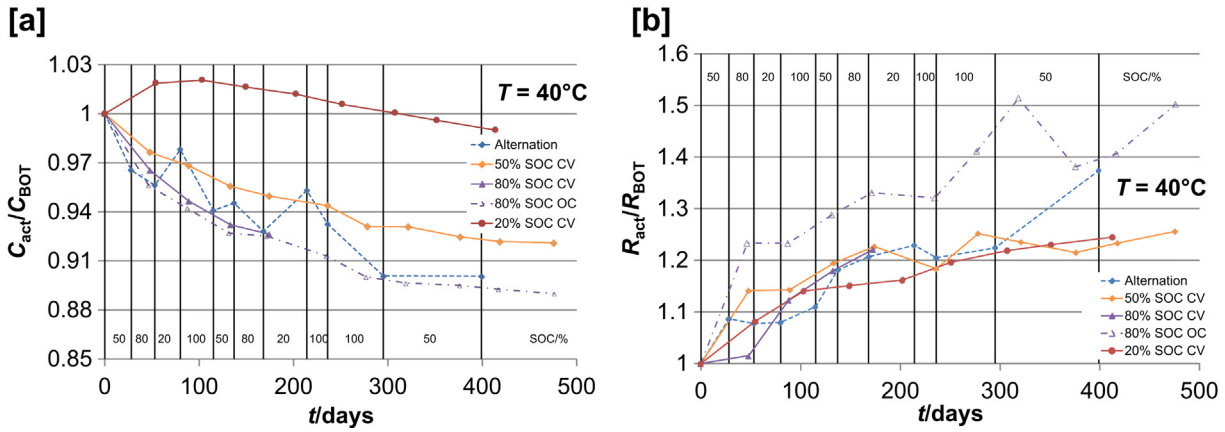

Fig. 15. Normalized actual capacity C_{act} (a) and resistance R_{act} (b) vs. time for calendar life scenarios at $T = 40\,^{\circ}C$. Alternation test with CV at changing SOC. Applied SOC profile values between RPTs are shown in the diagrams.

Table 4
Aging factors for capacity fade and resistance rise. For calculation the last set of values was used, where all voltages were still in test. E.g. a test at 100% SOC CV and $T = 40$ °C has a 3.8 times higher capacity loss than the 50% SOC CV test at the same temperature and time.

	Temperature	Related to SOC	SOC = 100% CV	SOC = 90% CV	SOC = 80% CV	SOC = 50% CV	SOC = 20% CV
C_{loss}	40 °C	50%	3.8	2	1.82	1	–
$R_{increase}$	40 °C	20%	2.0	1.6	1	1.2	1
C_{loss}	60 °C	20%	9.3	3	3	2.0	1
$R_{increase}$	60 °C	20%	8	1.2	1.52	1.4	1

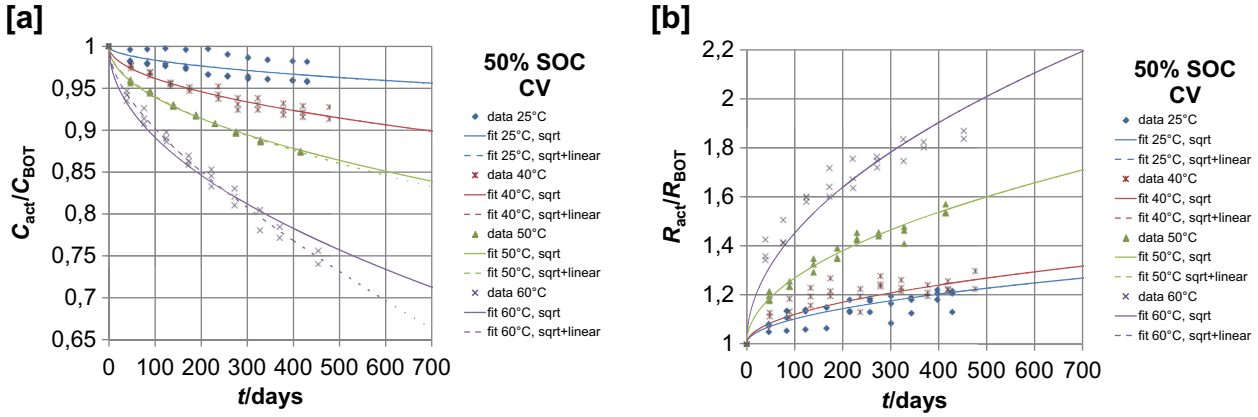

Fig. 16. Actual capacity C_{act} (a) and resistance R_{act} (b) over time for cells stored at 50% SOC at different temperatures. The dots show the measurement data for the each cell in test, the solid lines the fitting result using a single square root time behavior (eq. (3)) and the dashed lines depict the fitting result using a combination of square root and linear behavior for the time dependency (eq. (4)).

this method. Taking into account the curves at 100% SOC from the previous sections, the rise of resistance was expected to be high. In contrast the resistance in Fig. 15(b) during the 100% SOC periods does only lead to an at the most moderate resistance rise. One reason might be that such a simple model ignoring the previous history cannot be used in here. Also it cannot be excluded that parts of the curves behavior and difference to the aging curves next to the alternation test is due to scattering of the values.

3.7. Regression function and calendar lifetime extrapolation

Because strong hints point to the aforementioned processes on the anode side being the strongest aging effect, this is taken as working hypothesis in the following. In literature different theories can be found about the first principle processes of SEI growth during aging. As mentioned in the previous section, Broussely et al. describe in Ref. [4] the SEI forming at the SEI surface/electrolyte interface and therefore identify the electronic conductivity of the SEI as the rate limiting factor for SEI formation. Ploehn et al. [17] on the other hand identify the solvent diffusion process as the rate limiting factor. However, mathematical descriptions of both theories lead to the result that SEI formation has to follow a square root of time dependency. The capacity fade and resistance increase measured in this work support this theory. Similar to the work of Ecker et al. [3] in the following a function with square root of time dependency, as well as a combination of a square root and linear function have been fitted to the measured aging results:

$$\frac{A(t)}{A_{init}} = 1 \pm a_1 \cdot \sqrt{t} \tag{3}$$

$$\frac{A(t)}{A_{init}} = 1 \pm a_2 \cdot \sqrt{t} \pm b_2 \cdot t \tag{4}$$

A denotes cell capacity or resistance, respectively and a_1, a_2 and b_2 are constants determined by the fitting process. Fig. 16 shows the fitting results for capacity fade and resistance increase for cells stored at 50% SOC at different temperatures. In Table 5 the resulting fitting parameters and the corresponding correlation coefficients R^2 for capacity fade are given exemplarily. It can be seen, that a square root of time function describes the aging of the cells quite well. It can also be seen, that an additional linear term does not improve the fitting results significantly. Values for the linear fitting parameter b_2 of 10^{-4} to 10^{-14}show, that the linear contribution to aging is quite small and can be neglected in order to reduce the number of free parameters. Similar results can be found for the resistance. Therefore the square root function will be used in the following.

Based on the fitting results lifetime extrapolations can be calculated for the various test conditions. Fig. 17 shows capacity lifetime in (a), defined as the time, where capacity reaches 70% of initial capacity and resistive lifetime in (b) defined as the time, where the resistance reaches 200% of initial resistance over temperature at different SOC. At a moderate temperature of $T = 40$ °C the capacity lifetime ranges from 2 to 17 years depending on SOC. A cell stored at constant voltage of 4.18 V at $T = 40$ °C for example is only expected to live 2 years. Resistive lifetime is comparable to capacity lifetime for this special definition. At $T = 40$ °C resistive lifetime varies between 2 and 18 years for different SOC. At very moderate conditions like $T = 25$ °C and 50% SOC very high lifetimes can be reached according to the square root extrapolation. Capacity

Table 5
Fitting result for capacity fade for cells stored at 50% SOC and different temperatures. For the fitting eqs. (3) and (4) were used. The fitting parameters as well as the corresponding correlation coefficients R^2 are shown.

T [°C]	a_1	R^2	a_2	b_2	R^2
25	0.0017	0.9794	0.0016	3.8×10^{-6}	0.9813
40	0.0038	0.9885	0.0038	6.7×10^{-7}	0.9885
50	0.0061	0.9979	0.0057	2.24×10^{-5}	0.9994
60	0.0109	0.9802	0.0080	1.78×10^{-4}	0.9993

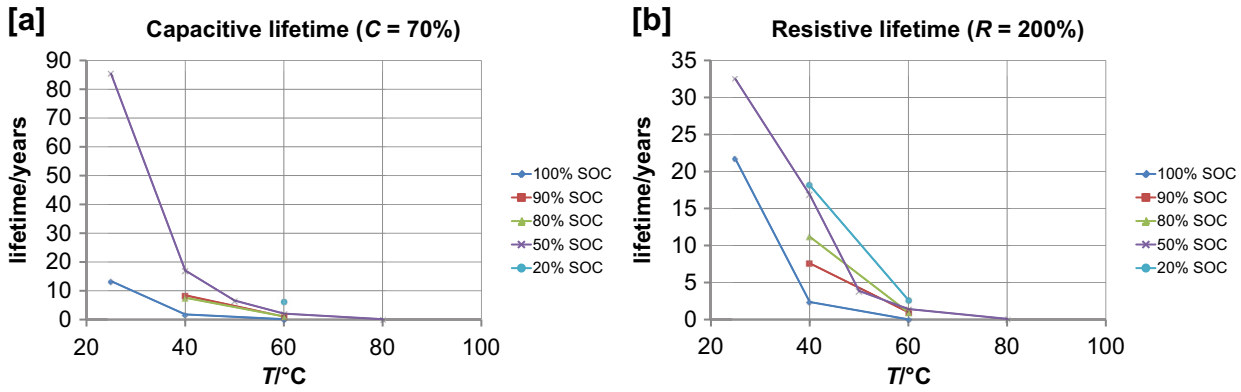

Fig. 17. Capacity lifetime (end of life (EOL) criterion: $C_{act} = 70\%\ C_{BOT}$) (a) and resistive lifetime (EOL criterion: $R_{act} = 200\%\ R_{BOT}$) vs. temperature for calendar life tests at different cell voltage levels.

lifetime becomes 85 years, resistive lifetime 32 years. One can argue that these numbers are not realistic, but it has to be kept in mind that the square root of time approach for the lifetime extrapolation only accounts for the internal aging mechanisms of SEI formation. All other aging mechanisms like leakage or loss of electrolyte e.g. caused by pouch bag rupture, or electrode irreversible loss due to active material degradation are not included in this approach. Furthermore, using a square root approach, scattering in the test data influences the predicted lifetime quite a lot. Neglecting the cell with lowest capacity degradation in the test with cells stored at 25 °C and 50% SOC at CV leads to a capacity lifetime of 56 years, in comparison to 85 years, if all three cells are considered in the fitting. In addition to the limitations on lifetime predictions mentioned before it has to be assured, that the aging influence is significantly higher than the scattering of the cells in one test set, which is mostly the case for higher temperatures leading to higher capacity loss and resistance increase. Using these accelerated aging tests has the disadvantage of possibly triggering aging processes which are unlikely to happen in real applications. These additional aging effects at higher temperatures would also invalidate the Arrhenius extrapolation of the test data to lower temperatures. If the mentioned limitations of this approach are considered, it can be used for lifetime estimation of high quality cells, where moderate SEI evolution is the main aging mechanism [13].

4. Conclusion

An extensive aging study of a graphite|$LiNi_{1/3}Mn_{1/3}Co_{1/3}O_2$ (NMC) Li-ion pouch cell has been presented in this work based on reference parameter tests to determine the aging behavior. Calendar life tests at different voltages and temperatures have been conducted as well as cycling tests at different average SOC and cycle depths. The temperature dependency could be identified as Arrhenius type and activation energies could be determined, which are in good accordance to the literature. The voltage dependency between 50% and 90% SOC is rather small. However, storing the cells at 20% SOC can be even beneficial for capacity, which can also be observed in a test with alternating voltage levels. This effect seems to be temperature independent. A comparison between calendar life aging at OC and CV showed significant differences only at 100% SOC in capacity decline. This is caused by the relative small dependency of the aging on cell voltage below 100% SOC. Therefore deviations from the set lower SOC in the OC tests due to self-discharge are of minor importance. SEI formation on the anode is expected to be the main aging mechanism for calendar life tests, causing a square root of time shaped aging behavior.

The aging behavior of cycling tests has been identified as dependent on temperature and cycle depth. Cycling tests at 10% DOD show a capacity decline equal to calendar life aging tests. Higher DOD (50% and full cycling) led to increased additional capacity fade. A complex impact of cycling on resistance increase has been observed. At $T = 25$ °C and high DOD there was even a smaller resistance increase than in the corresponding calendar life test. Taking results from post-mortem analysis from paper part B into account, the resistance for cyclic aging appears to be depended on the interaction of volume increase and deposition reactions on the anode side. Further studies including post-mortem analysis in paper part B and EIS will be presented in separate publications for clarification of the occurring aging effects. More data and an in-depth analysis of the cycling tests will follow as well.

Acknowledgments

This work was sponsored by the German Federal Ministry of Education and Research (BMBF) under contract no. 03X4613G as part of the program “LIB 2015”. The authors are grateful to Continental and Daimler for their assistance to this study as partners of this project. Special thanks go to ZSW for providing results from post-mortem analysis.

References

[1] M. Wachtler, M. König, M. Kasper, M. Fleischhammer, B. Emmermacher, P. Axmann, M. Wohlfahrt-Mehrens, J. Power Sources, submitted for publication.
[2] M. Safari, M. Morcrette, A. Teyssot, C. Delacourt, J. Electrochem. Soc. 156 (2009) A145–A153.
[3] M. Ecker, J.B. Gerschler, J. Vogel, S. Käbitz, F. Hust, P. Dechent, D.U. Sauer, J. Power Sources 215 (2012) 248–257.
[4] M. Broussely, S. Herreyre, P. Biensan, P. Kasztejna, K. Nechev, R. Staniewicz, J. Power Sources 97–98 (2001) 13–21.
[5] G. Ning, B. Haran, B.N. Popov, J. Power Sources 117 (2003) 160–169.
[6] J. Shim, K.A. Striebel, J. Power Sources 122 (2003) 188–194.
[7] R. Wright, C. Motloch, J. Belt, J. Christophersen, C. Ho, R. Richardson, I. Bloom, S. Jones, V. Battaglia, G. Henriksen, T. Unkelhaeuser, D. Ingersoll, H. Case, S. Rogers, R. Sutula, J. Power Sources 110 (2002) 445–470.
[8] I. Bloom, B. Cole, J. Sohn, S. Jones, E. Polzin, V. Battaglia, G. Henriksen, C. Motloch, R. Richardson, T. Unkelhaeuser, D. Ingersoll, H. Case, J. Power Sources 101 (2001) 238–247.
[9] J. Wang, P. Liu, J. Hicks-Garner, E. Sherman, S. Soukiazian, M. Verbrugge, H. Tataria, J. Musser, P. Finamore, J. Power Sources 196 (2011) 3942–3948.
[10] M. Kassem, J. Bernard, R. Revel, S. Pélissier, F. Duclaud, C. Delacourt, J. Power Sources 208 (2012) 296–305.
[11] I. Bloom, L.K. Walker, J.K. Basco, D.P. Abraham, J.P. Christophersen, C.D. Ho, J. Power Sources 195 (2010) 877–882.

[12] J. Vetter, P. Novák, M. Wagner, C. Veit, K.-C. Möller, J. Besenhard, M. Winter, M. Wohlfahrt-Mehrens, C. Vogler, A. Hammouche, J. Power Sources 147 (2005) 269–281.
[13] M. Broussely, P. Biensan, F. Bonhomme, P. Blanchard, S. Herreyre, K. Nechev, R. Staniewicz, J. Power Sources 146 (2005) 90–96.
[14] P. Verma, P. Maire, P. Novák, Electrochim. Acta 55 (2010) 6332–6341.
[15] J.B. Goodenough, Y. Kim, Chem. Mater. 22 (2010) 587–603.
[16] P. Novák, F. Joho, M. Lanz, B. Rykart, J.-C. Panitz, D. Alliata, R. Kötz, O. Haas, J. Power Sources 97–98 (2001) 39–46.
[17] H.J. Ploehn, P. Ramadass, R.E. White, J. Electrochem. Soc. 151 (2004) A456–A462.
[18] B.Y. Liaw, E. Roth, R.G. Jungst, G. Nagasubramanian, H.L. Case, D.H. Doughty, J. Power Sources 119–121 (2003).
[19] J.R. Dahn, Phys. Rev. B 44 (1991) 9170–9177.
[20] Y.-G. Ryu, S. llPyun, J. Electroanal. Chem. 433 (1997) 97–105.